Journal of Thermal Engineering
Web page info: https://jten.yildiz.edu.tr
DOI: 10.14744/jten.2021.xxxx

Research Article

Influence of Convective Boundary Condition on heat and mass transfer in a Walters' B fluid over a vertical stretching surface with thermal-diffusion effect

B.J. AKINBO¹* , **B.I. OLAJUWON¹**

¹Department of Mathematics, Federal University of Agriculture, Abeokuta, Nigeria

ARTICLE INFO

ABSTRACT

This paper presents the influence of Convective Boundary Condition on heat and mass transfer in a Walters' B fluid over a vertical stretching sheet with the thermal-diffusion effect. The coupled nonlinear partial differential equations governing the system are presented in the form of coupled ordinary differential equations via similarity transformation variables which then solved by the Homotopy Analysis Method. The effect of various parameters on velocity, temperature and concentration profiles as well as Local Skin-friction, Nusselt and Sherwood numbers are plotted and discussed. The result shows among others that large values of the thermal buoyancy parameter accelerate the motion of the fluid and cools the thermal layer while the surface heat transfer is boosted when the strength of Radiation improves. Also, large values of Biot number constitute strong convective heating which consequently maximizes thermal boundary layer thickness and paves way for the penetration of thermal effect to the quiescent fluid. Biot number is of great importance in the engineering field for drying of the materials.

Cite this article as: B.J. Akinbo, B.I. Olajuwon. Influence of Convective Boundary Condition on heat and mass transfer in a Walters' B fluid over a vertical stretching surface with thermal-diffusion effect. J Ther Eng 2021;7(7):1784–1796.

INTRODUCTION

The interaction of heat and mass transfer by natural convection in laminar boundary layer flows has received significant attention in the years past and extensively studied in the literature for both steady and unsteady phenomenon of Newtonian fluid due to its numerous applications in science and engineering field. Among the early

investigation revealed by Ali et'al. [1] shows that thermal radiation interaction enhances the wall shear stress as well as the surface heat transfer rate while investigating the natural convection-radiation interaction in boundary layer flow over the horizontal surface. Arpaci [2] studied the effect of thermal radiation on the laminar free convection from a

*Corresponding author.
*E-mail address: bjakinbo@fce-abeokuta.edu.ng

This paper was recommended for publication in revised form by Regional Editor Omid Mahian

heated vertical plate. Recently, other researchers also made their contribution to the literature. Afify and El-Aziz [3] revealed that the heat transfer rates for both pseudoplastic and dilatant nano fluids are insensitive to change in viscosity for lower values of Biot number and declined by relatively strong convective heating with higher values of Biot number. Sarafraz et'al. [4] reported that the only influence of sub-cooling temperature is found to decrease the corresponding heat flux related to the onset of nucleate boiling. El-Aziz and Nabil [5] justified among others that the velocity slip leads to a faster rate of cooling of the stretching sheet only in the case of free convection flow regime. El-Aziz [6] investigated thermal-diffusion and diffusion-thermo effects on combined heat and mass transfer by hydromagnetic three-dimensional free convection over a permeable stretching surface with radiation. The result shows among others that the maximum effect of the thermal-diffusion and diffusion-thermo on the velocity occurs in the absence of the magnetic field when the plate is impermeable. El-Aziz [7] examined the radiation effect on the flow and heat transfer over an unsteady stretching sheet where it was pointed out that the effect of radiation parameter on the temperature distribution of a steady flow is more pronounced than that of unsteady flow. Abo-Eldahab and El Aziz [8] investigated the effect of blowing/suction on hydromagnetic heat transfer by mixed convection from an inclined continuously stretching surface with internal heat generation/absorption. Oahimire and Olajuwon [9] examined the effect of radiation absorption and thermo-diffusion on MHD heat and mass transfer flow of a micropolar fluid in the presence of heat source. The result shows among others that in the presence of the uniform magnetic field, an increase in the strength of the applied magnetic field decelerates the fluid motion along the wall of the plate inside the boundary layer, whereas the micro-rotational velocity of the fluid along the wall of the plate increase. Makinde [10] reported the effect of heat and mass transfer on MHD over a moving vertical plate with a convective boundary condition. However, the law of Newtonian fluid has been proved to be in good agreement with Newton's second law of motion which work very well for air, water and other fluid delineated with Navier-Stokes and conservation of energy equation but failed while dealing with more complex fluid, especially with the emergence of viscoelastic fluid or polymeric liquid. The deficiency encountered in the theory of Newtonian fluid and recent development in Science and Technology with its numerous biological and industrial applications, such as polymer solution, paint ink, and cake butter e.t.c had made its studies interesting to all and recently studied in the literature. El-Aziz [11] found that a viscoelastic fluid is more sensitive to the variable fluid properties effect than a Newtonian fluid. Labropulu et'al. [12] examined the stagnation-point flow of the Walters' B fluid with slip where the effect of condition and the viscoelasticity were to increase the velocity near the wall. Shivakumara et'al. [13] reported that the effect of thermal modulation disappears at large frequencies in all the cases of thermal modulation while investigating the effect of thermal modulation on the onset of convection in Walters B viscoelastic fluid-saturated porous medium. Rana et'al. [14] and (Aggarwal and Verma [15]) reported that Walters' (model B') visco-elastic fluid behaves like an ordinary Newtonian fluid due to the vanishing of the visco-elastic parameter. Pandey et'al. [16] investigated the characteristic of Walter's B visco-elastic Nanofluid layer heated from below. It is reported among other that the Kinematic visco-elasticity parameter destabilizes the oscillatory convection and no has effects on stationary convection. Other authors like Thirumurugan and Vasanthakumari [17], Sharma et' al. [18], Kango et'al. [19], Rana [20–21] also contributed to the literature about Walters' B fluid.

Going by the previous effort of other researchers in the literature, much attention has not been given to the impact of the Boit number on Walters' B fluid. On that note, this work is set to examine the influence of Convective Boundary Condition on heat and mass transfer in a Walters' B fluid over a vertical stretching surface with thermal-diffusion effect, having considered unaddressed to the best of our knowledge in the literature. The boundary layer equations governing the system are then solved via the Homotopy Analysis Method being a modern method for solving both linear and nonlinear differential equations.

MATHEMATICAL FORMULATION

In this article, the steady flow of heat and mass transfer over a vertical surface of Walters' B viscoelastic fluid is considered. We assumed that the plate experienced heat by convection at a temperature T_f which provides heat transfer coefficient h_f. A magnetic field B_0 of uniform strength is executed in y-direction while the induced magnetic field is not taken into account due to the magnetic Reynolds number that is really small in the most fluid used in industries and the joule heating is neglected as it really small to affect the motion of free convection. The *x-axis* is taken along the direction of the main flow and *y-axis* normal to it. The temperature and concentration of the fluid is respectively considered as T and C, C_w is the plate surface concentration while T_∞ and C_∞ respectively denote the ambient temperature and concentration. The heat and mass transfer characteristics areconsidered in the presence of non-uniform heat generation/absorption and thermal-diffusion effect. (See Fig. 1). The stretching sheet is moving with a velocity $u_w(x) = ax$ and $a > 0$.

On the account of elastic properties of the fluid which are important in extensional behaviors of polymer, the stress tensor S^* for Walters' B fluid is expressed as (See Nadeem et'al. [22]);

$$S^\star = 2\eta_0 - 2k_0 \frac{\delta e}{\delta t} \tag{1}$$
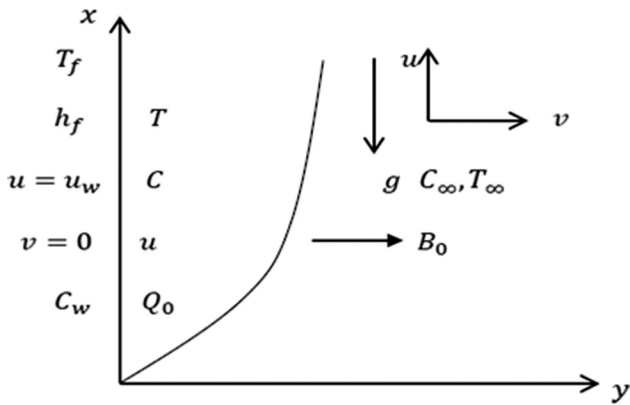
Figure 1. Flow configuration and coordinate system.

where e is the rate of strain tensor and $\dfrac{\delta e}{\delta t}$ is the convected derivative of a tensor quantity in relation to the material motion, expressed as $\dfrac{\delta e}{\delta t} = \dfrac{\partial e}{\partial t} + v.\nabla e - e\nabla V - (\nabla V)^T.e$, $\eta_0 = \int_0^\infty N(\tau)d\tau$ denotes the limiting viscosity at small shear rates, $k_0 = \int_0^\infty \tau N(\tau)d\tau$ represents the short memory coefficient, while $N(\tau)$ is the distribution function with relaxation time τ. Keeping in mind the short memory, the term involving $k_0 = \int_0^\infty \tau^n N(\tau)d\tau$ (at $n \geq 2$) is neglected. On the account of the assumption stated above and under usual Boussinesq's approximation, the governing equation for Walters' B fluid, in agreement with Mihra et' al. [23] is given by

$$\frac{\partial u}{\partial x} + \frac{\partial v}{\partial y} = 0 \tag{2}$$

$$u\frac{\partial u}{\partial x} + v\frac{\partial u}{\partial y} = v\frac{\partial^2 u}{\partial y^2} -$$
$$k_0\left[u\frac{\partial^3 u}{\partial x\partial y^2} + v\frac{\partial^3 u}{\partial y^3} + \frac{\partial u}{\partial x}\frac{\partial^2 u}{\partial y^2} - \frac{\partial u}{\partial y}\frac{\partial^2 u}{\partial x\partial y}\right] \tag{3}$$
$$-\frac{\sigma B_0^2 u}{\rho} + g\beta_T(T - T_\infty) + g\beta_c(C - C_\infty)$$

$$u\frac{\partial T}{\partial x} + v\frac{\partial T}{\partial y} = \alpha\frac{\partial^2 T}{\partial y^2} - \frac{1}{\rho C_\rho}\frac{\partial qr}{\partial y} + Q_0 \tag{4}$$

$$u\frac{\partial C}{\partial x} + v\frac{\partial C}{\partial y} = D_m\frac{\partial^2 C}{\partial y^2} + \frac{D_m K_T}{T_m}\frac{\partial^2 T}{\partial y^2} \tag{5}$$

The appropriate boundary conditions for the problem are expressed as

$$u(x,0) = u_w(x) = ax, v(x,0) = 0, -k\frac{\partial T(x,0)}{\partial y}$$

$$= h_f[T_f - T(x,0)], C(x,0) = C_w$$
$$U(x,\infty) = 0, T(x,\infty) = T_\infty, C(x,\infty) = C_\infty \tag{6}$$

The velocity components acting in x and y directions are respectively denoted as u and v, q_r is the radiation heat flux, C_p is the specific heat at constant pressure, v is the kinematic viscosity, β_c is the concentration expansion coefficient, D_m is the mass diffusivity, α is the thermal diffusivity, g is the acceleration due to gravity, ρ is the density, T_m is the mean fluid temperature, σ is the fluid electrical conductivity, K_T is the thermal diffusion ratio, Q_0 is the non-uniform heat generation/absorption coefficient defined by $Q_0 = \dfrac{ku_w(x)}{\rho C_\rho xv}[A(T_w - T_\infty)f' + (T - T_\infty)B]$, where A connotes the space-dependent and B stands for the temperature-dependent heat generation/absorption (see Hayat et' al. [24]) while β_T is the thermal expansion coefficient. Keeping in mind that the boundary layer is optically thick, therefore, the Rosseland approximation for heat transfer is considered (See Uddin et'al. [25]), hence, the radiative heat flux is modeled as

$$qr = \frac{-4\sigma^\star}{3k^\star}\frac{\partial T^4}{\partial y} \tag{7}$$

where $k^\star$ is the means of absorption coefficient and $\sigma^\star$ is the Sterfan-Boltzmann constant. We assumed that the temperature variation within the flow is such that the term T^4 may be simplified as a linear function of temperature by expanding T^4 in a Taylor series about T_∞ and neglecting higher-order terms, gives

$$T^4 \approx 4T_\infty^3 T - 3T_\infty^4 \tag{8}$$

invoking (7) and (8) in equation (3), gives a modified equation of the form

$$u\frac{\partial T}{\partial x} + v\frac{\partial T}{\partial y} = \alpha\frac{\partial^2 T}{\partial y^2} + \frac{16\sigma^\star T_\infty^3}{3k^\star \rho C_\rho}\frac{\partial^2 T}{\partial y^2} + Q_0 \tag{9}$$

The continuity equation (2) is automatically satisfied by the application of the stream function ψ defined by

$$u = \frac{\partial \psi}{\partial y} \quad \text{and} \quad v = -\frac{\partial \psi}{\partial x} \tag{10}$$

In accordance with Almakki et'al. [26], the similarity solution for momentum, energy and concentration equations are obtained by the application of the appropriate transformation method defined as

$$\eta = y\sqrt{\frac{a}{v}}, \ \psi = x\sqrt{av}f(\eta),$$
$$\theta(\eta) = \frac{T - T_\infty}{T_f - T_\infty}, \ \phi(\eta) = \frac{C - C_\infty}{C_W - C_\infty} \tag{11}$$

Here, η denotes independent similarity variable, $\theta(\eta)$ and $\phi(\eta)$ are dimensionless temperature and concentration respectively. Introducing (10) and (11) in (3), (9) and (5), result in

$$f'''(\eta) + f(\eta)f''(\eta) - (f'(\eta))^2 + \beta[(f''(\eta))^2 - 2f'(\eta)f'''(\eta) + f(\eta)f^{(iv)}(\eta)]$$
$$-Mnf'(\eta) + \lambda_T\theta(\eta) + \lambda_M\phi(\eta) = 0 \qquad (12)$$

$$\left(1 + \frac{4}{3}Ra\right)\theta''(\eta) + \Pr f(\eta)\theta'(\eta)$$
$$+ Af'(\eta) + B\theta(\eta) = 0 \qquad (13)$$

$$\phi''(\eta) + Scf(\eta)\phi'(\eta) + Sr\theta''(\eta) = 0 \qquad (14)$$

satisfying the following boundary conditions

$$f(0) = 0, f'(0) = 1, \theta'(0) = Bi[\theta(0) - 1], \phi(0) = 1 \quad (15)$$

$$f'(\infty) = 0, \theta(\infty) = 0, \phi(\infty) = 0 \qquad (16)$$

where the prime symbol denotes the derivate with respect to η, $Mn = \dfrac{\sigma B_0^2}{\rho a}$ is the magnetic field, $\beta = \dfrac{ak_0}{\nu}$ is the local Weissenberg Number, $\lambda_T = \dfrac{Gr_x}{(Re_x)^2}$ is the thermal buoyancy parameter, $\lambda_M = \dfrac{Gc_x}{(Re_x)^2}$ is the mass buoyancy parameter, $Gr_x = \dfrac{g\beta_T(T_W - T_\infty)x^3}{\nu^2}$ is the thermal Grash of Number, $Gc_x = \dfrac{g\beta_C(C_W - C_\infty)x^3}{\nu^2}$ is the solutal Grashof Number, $Bi = \dfrac{h_f}{k}\sqrt{\dfrac{\nu}{a}}$ is the Biot number, $Re_x = \dfrac{u(x)}{\nu}$ is the Relyold Number, $Pr = \dfrac{\nu\rho Cp}{k}$ is the prandtl number, $Ra = \dfrac{4\sigma^\star T_\infty^3}{kk^\star}$ is the radiation parameter, $Sr = \dfrac{K_T(T_f - T_\infty)}{T_m(C_w - C_\infty)}$ is the Soret number, $Sc = \dfrac{\nu}{D_m}$ is the Schmidtl number.

Keeping in mind the engineering application of the study, the local skin friction coefficient, the local Nusselt number, and the Local Sherwood number are respectively presented in the form

$$C_f = \frac{2\tau_w}{\rho u_w^2}, \ Nu = \frac{xq_w}{k(T_w - T_\infty)},$$
$$Sh = \frac{xq_m}{D_m(C_w - C_\infty)} \qquad (17)$$

Where

$$\tau_w = \left[\mu\frac{\partial u}{\partial y} - k_0\left(u\frac{\partial^2 u}{\partial x\partial y} + v\frac{\partial^2 u}{\partial y^2} + 2\frac{\partial u}{\partial x}\frac{\partial v}{\partial y}\right)\right]_{y=0},$$
$$q_w = \left[-k\frac{\partial T}{\partial y}\right]_{y=0} = \left[-\frac{4\sigma}{3K^\star}\frac{\partial T^4}{\partial y}\right]_{y=0}, \qquad (18)$$
$$q_m = \left[-D_m\frac{\partial C}{\partial y}\right]_{y=0}$$

By the introduction of (18) in (17) with the above transformation technique, an expression for local Skin-friction, the local Nusselt number, and the local Sherwood number formulated and given as

$$Re_x^{\frac{1}{2}}C_f = (1 - \beta)f''(0), \ Re_x^{-\frac{1}{2}}Nu = -\left(1 + \frac{4}{3}Ra\right)\theta'(0),$$
$$Re_x^{-\frac{1}{2}}Sh = \phi'(0) \qquad (19)$$

where $Re_x = u_w(x)/\nu$ represents the Reynold number, τ_w is the shear stress along with the plate, q_w is the surface heat and q_m is the surface mass.

HOMOTOPY ANALYSIS METHOD

The solution of the differential equation has been the utmost priority of every researcher in mathematical modeling. They are solved by different methods among which are Shooting Techniques with Runge-Kutta method, Variation iteration method and Weighted Residual Method e.t.c. Homotopy Analysis Method is chosen and used over other methods being a modern Method and very efficient in solving both bounded and unbounded domain of differential equations. Subject to the rule of the solution and boundary conditions (15) – (16), we choose the initial guess (See Hayat et'al. [24], and Liao [27])

$$f_0(\eta) = 1 - \exp(-\eta), \ \theta_0(\eta) = \frac{Bi\,\exp(-\eta)}{(1 + Bi)},$$
$$\phi_0(\eta) = \exp(-\eta) \qquad (20)$$

as the initial linear approximations of $f(\eta)$, $\theta(\eta)$ and $\phi(\eta)$. The auxiliary linear operations L_f, L_θ, and L_ϕ are;

$$L_f[f(\eta;r)] = \frac{\partial^3 f(\eta;r)}{\partial\eta^3} - \frac{\partial f(\eta;r)}{\partial\eta},$$
$$L_\theta[\theta(\eta;r)] = \frac{\partial^2\theta(\eta;r)}{\partial\eta^2} - \theta(\eta;r), \qquad (21)$$
$$L_\phi[(\eta;r)] = \frac{\partial^2\phi(\eta;r)}{\partial\eta^2} - \phi(\eta;r)$$

Satisfied the following properties

$$L_f[C_1 + C_2\ exp(\eta) + C_3\ exp(-\eta)] = 0,$$
$$L_\theta[C_4 + C_5\ exp(-\eta)] = 0, L_\phi[C_6 + C_7\ exp(-\eta)] = 0 \quad (22)$$

where $C_1, C_2, ..., C_7$ are constants.

ZERO ORDER DEFORMATION PROBLEM.

$$(1-r)L_f[f(\eta;r) - f_0(\eta)] = r\hbar_f H_f(\eta)N_f[f(\eta;r),$$
$$\theta(\eta;r), \phi(\eta;r)] \quad (23)$$

$$(1-r)L_\theta[f(\eta;r) - \theta_0(\eta)] = r\hbar_\theta H_\theta(\eta)N_\theta[f(\eta;r), \theta(\eta;r)] \quad (24)$$

$$(1-r)L_\phi[f(\eta;r) - \phi_0(\eta)] = r\hbar_\phi H_\phi(\eta)N_\phi[f(\eta;r),$$
$$\theta(\eta;r), \phi(\eta;r)] \quad (25)$$

where L and N are called Linear and non-linear function respectively (for Algebra Equation) or Linear and Non-linear operators (for differential Equations) and $r\in[0,1]$ is the embedding parameter, with the following boundary conditions (See Akinbo and Olajuwon [28]).

$$f(\eta = 0;r) = 0, \quad \frac{\partial f(\eta;r)}{\partial \eta}\Big|_{\eta=0} = 1,$$

$$\frac{\partial \theta(\eta;r)}{\partial \eta}\Big|_{\eta=0} = Bi[\theta(\eta = 0;r) - 1], \quad (26)$$

$$\phi(\eta = 0;r) = 1$$

$$\frac{\partial f(\eta;r)}{\partial \eta}\Big|_{\eta\to 0} = 0, \ \theta(\eta\to\infty;r) = 0 = \phi(\eta\to\infty;r) \quad (27)$$

The nonlinear operators N_f, N_θ, and N_ϕ are defined as

$$\frac{\partial^3 f(\eta;r)}{\partial \eta^3} + f(\eta;r)\frac{\partial^2 f(\eta;r)}{\partial \eta^2} - \left(\frac{\partial f(\eta;r)}{\partial \eta}\right)^2 -$$
$$\beta\left[2\frac{\partial f(\eta;r)}{\partial \eta}\frac{\partial^2 f(\eta;r)}{\partial \eta^2} -\right.$$
$$\left. f(\eta;r)\frac{\partial^4 f(\eta;r)}{\partial \eta^4} - \left(\frac{\partial^2 f(\eta;r)}{\partial \eta^2}\right)^2\right] \quad (28)$$
$$- Mn\frac{\partial f(\eta;r)}{\partial \eta} + \lambda_T\theta(\eta;r) + \lambda_m\phi(\eta;r) = 0$$

$$\left[1 + \frac{4}{3}Ra\right]\frac{\partial^2\theta(\eta;r)}{\partial \eta^2} + Pr\frac{\partial\theta(\eta;r)}{\partial \eta}f(\eta;r) +$$
$$A\frac{\partial f(\eta;r)}{\partial \eta} + B\theta(\eta;r) = 0 \quad (29)$$

$$\frac{\partial^2\phi(\eta;r)}{\partial \eta^2} + Scf(\eta;r)\frac{\partial\phi(\eta;r)}{\partial \eta} + Sr\frac{\partial^2\theta(\eta;r)}{\partial \eta^2} = 0 \quad (30)$$

where $r\in[0,1]$ is the same as the embedding parameter defined above. The increase in embedding parameter r from Zero to One corresponds to a variation of the function $f(\eta;r)$, $\theta(\eta;r)$ and $\phi(\eta;r)$ from initial guess $f_0(\eta)$, $\theta_0(\eta)$ and $\phi_0(\eta)$ to the solutions $f(\eta)$, $\theta(\eta)$ and $\phi(\eta)$. Using Taylor series with respect to r, we have

$$f(\eta;r) = f_0(\eta) + \sum_{m=1}^{\infty} f_m(\eta)r^m,$$
$$\theta(\eta;r) = \theta_0(\eta) + \sum_{m=1}^{\infty} \theta_m(\eta)r^m, \quad (33)$$
$$\phi(\eta;r) = \phi_0(\eta) + \sum_{m=1}^{\infty} \phi_m(\eta)r^m$$

where $f_m(\eta) = \frac{1}{m!}\frac{\partial^m f(\eta;r)}{\partial \eta^m}$, $\theta_m(\eta) = \frac{1}{m!}\frac{\partial^m\theta(\eta;r)}{\partial\theta^n}$,

$$\phi_m(\eta) = \frac{1}{m!}\frac{\partial^m\phi(\eta;r)}{\partial\phi^m}$$

Obviously, the convergence of the series (33) is subject to the auxiliary parameter $\hbar$. Assuming $\hbar$ is chosen such that the series (33) converge at $r = 1$, we have

$$f(\eta) = f_0(\eta) + \sum_{m=1}^{\infty} f_m(\eta),$$
$$\theta(\eta) = \theta_0(\eta) + \sum_{m=1}^{\infty} \theta_m(\eta), \quad (34)$$
$$\phi(\eta) = \phi_0(\eta) + \sum_{m=1}^{\infty} \phi_m(\eta)$$

Mth-ORDER DEFORMATION PROBLEM

Following Hayat et'al. [29], the mth-order deformation are considered as follow

$$L_f[f_m(\eta) - \chi_m f_{m-1}(\eta)] = \hbar R_m^f(\eta),$$
$$L_\theta[\theta_m(\eta) - \chi_m\theta_{m-1}(\eta)] = \hbar R_m^\theta(\eta)$$
$$L_\phi[\phi_m(\eta) - \chi_m\phi_{m-1}(\eta)] = \hbar R_m^\phi(\eta) \quad (35)$$

having the following boundary conditions.

$$f_m(\eta = 0;0) = 0, \frac{\partial f_m(\eta = 0;0)}{\partial \eta} = 0, \frac{\partial\theta_m(\eta = 0;0)}{\partial \eta} =$$
$$Bi[\theta_m(\eta = 0;0)], \phi_m(\eta = 0;0) = 0 \quad (36)$$

$$\frac{\partial f_m(\eta\to\infty)}{\partial \eta} = 0, \ \theta_m(\eta\to\infty) = 0 = \phi_m(\eta\to\infty) \quad (37)$$

Where

$$R_m^f(\eta) = \frac{d^3 f_{m-1}(\eta)}{d\eta^3} + \sum_{n=0}^{m-1} f_n(\eta) \frac{d^2 f_{m-1-n}(\eta)}{d\eta^2} -$$
$$\sum_{n=0}^{m-1} \frac{df_n(\eta)}{d\eta} \frac{df_{m-1-n}(\eta)}{d\eta} - 2\beta\eta \frac{d^2 f_{m-1-n}(\eta)}{d\eta^2}$$
$$+ \beta \sum_{n=0}^{m-1} f_n(\eta) \frac{d^4 f_{m-1-n}(\eta)}{d\eta^4} + \qquad (38)$$
$$\beta \sum_{n=0}^{m-1} \frac{d^2 f_n(\eta)}{d\eta^2} \frac{d^2 f_{m-1-n}(\eta)}{d\eta^2} -$$
$$Mn \frac{df_{m-1}(\eta)}{d\eta} + \lambda_T \theta_{m-1}(\eta) + \lambda_M \phi_{m-1}(\eta)$$

$$R_m^\theta(\eta) = \left[1 + \frac{4}{3} Ra\right] \frac{d^2 \theta_{m-1}(\eta)}{d\eta^2} +$$
$$Pr \sum_{n=0}^{m-1} f_n(\eta) \frac{d\theta_{m-1-n}(\eta)}{d\eta} + \qquad (39)$$
$$A \frac{df_{m-1}(\eta)}{d\eta} Q\theta_{m-1}(\eta)$$

$$R_m^\phi(\eta) = \frac{d^2 \phi_{m-1}(\eta)}{d\eta^2} + Sc \sum_{n=0}^{m-1} f_n(\eta) \frac{d\phi_{m-1-n}(\eta)}{d\eta} +$$
$$Sr \frac{d^2 \theta_{m-1}(\eta)}{d\eta^2} \qquad (40)$$

and $\chi_m = 0$ for $m \le 1$, $\chi_m = 1$ for $m > 1$
having the following as a general solution

$$f_m(\eta) = f_m^*(\eta) + C_1 + C_2 exp(-\eta) + C_3 exp(-\eta) \qquad (41)$$

$$\theta_m(\eta) = \theta_m^*(\eta) + C_4 + C_5 exp(\eta) \qquad (42)$$

$$\phi_m(\eta) = \phi_m^*(\eta) + C_6 + C_7 exp(\eta) \qquad (43)$$

where $f_m^*(\eta)$, $\theta_m^*(\eta)$ and $\phi_m^*(\eta)$ represent the particular solution of equation (35). In agreement with Olubode et'al.
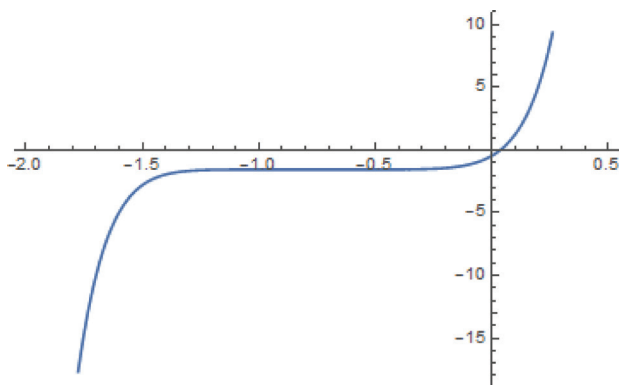
[30], we consider the rule of coefficient ergodicity and rule of solution existence and choose the auxiliary functions as

$$H_f = H_\theta = H_\phi = 1$$

CONVERGENCE OF THE HAM SOLUTION

The convergence solution of this present investigation is considered in line with Liao [31], Akinbo and Olajuwon [28] suggestions. The non-zero auxiliary parameters $\hbar_f$, $\hbar_\theta$ and $\hbar_\phi$ help to monitor and control the convergence of the series solution. By the application of the following parameters $Bi = \lambda_T = Sr = \lambda_M = \beta = 0.1$, $Sc = 0.62$, $Pr = 0.72$, $Ra = 0.7$, $Mn = 1$, $A = B = 0.01$. The admissible values of $\hbar_f$, $\hbar_\theta$ and $\hbar_\phi$ are presented at the range where $\hbar - curve$ becomes parallel which in turns give $-1.2 \le \hbar_f \le -0.3$, $-1.3 \le \hbar_\theta \le -0.4$ and $-1.5 \le \hbar_\phi \le -0.4$ for $\hbar_f$, $\hbar_\theta$ and $\hbar_\phi$ respectively as demonstrated in figures (2–4) below

The exact approximate solution for the convergence of the governing equations which corresponds to momentum, energy and concentration equations are presented in table 1. The dimensionless equations meet the far-field domains and the iteration series converges at $20th - order$
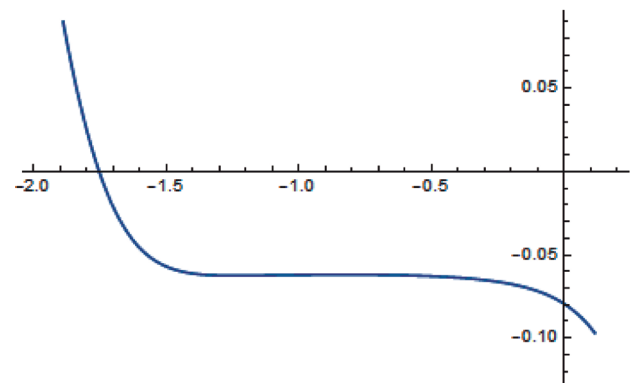
Figure 3. $\hbar_\theta$ – curve of $\theta'(0)$ at 10th approximation.

Figure 2. $\hbar_f$ – curve of $f''(0)$ at 10th approximation.
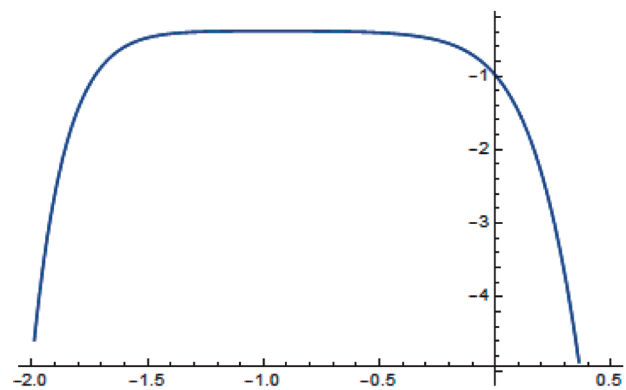
Figure 4. $\hbar_\phi$ curve of $\phi'(0)$ at 10th approximation.

Table 1. Convergence of solution

Order of Approximation	$f''(0)$	$-\theta'(0)$	$-\phi'(0)$
5	−1.0183	0.0767	0.4284
10	−1.0126	0.0741	0.4195
12	−1.0118	0.0737	0.4193
14	−1.0112	0.0733	0.4196
16	−1.0110	0.0731	0.4199
18	−1.0108	0.0729	0.4202
20	−1.0106	0.0728	0.4205
22	−1.0106	0.0727	0.4205
24	−1.0106	0.0727	0.4205

for momentum and concentration equations while the energy equation converges at $22th - order$ of iterations while table 2 agreed with Hayat et'al.[24]. However, the results are validated using Galerkin Weighted Residual

Table 2. Validation with Hayat et'al.[24] at $Mn = 0$, $\lambda_T = 0$, $\lambda_M = 0$

Parameter		Hayat et'al.[24]	Present Result
S	β	$^-Re_x^{\frac{1}{2}}C_f$	$^-Re_x^{\frac{1}{2}}C_f$
0.0	0.2	0.870726	0.87072581

Table 3. Validation/Numerical result for local Skin-friction coefficient, Local Nusselt number, and Local Sherwood number

Parameters											Results with HAM			Results with Galerkin Weighted Residual Method		
β	Mn	λ_T	λ_M	Pr	Sc	Bi	Sr	Ra	A	B	$Re_x^{\frac{1}{2}}C_f$	$Re_x^{\frac{1}{2}}Nu$	$Re_x^{\frac{1}{2}}Sh$	$Re_x^{\frac{1}{2}}C_f$	$Re_x^{\frac{1}{2}}Nu$	$Re_x^{\frac{1}{2}}Sh$
0.1	0.1	0.1	0.1	0.72	0.62	0.1	0.1	0.7	0.01	0.01	−0.90956	0.14076	0.42049	−0.90955	0.14075	0.42046
0.3											−0.80862	0.13897	0.40152	−0.80861	0.13895	0.40150
0.5											−0.77412	0.13644	0.38047	−0.77410	0.13643	0.38045
	1.0										−1.27062	0.13497	0.35813	−1.27061	0.13495	0.35811
	2.0										−1.58216	0.13101	0.31603	−1.58215	0.13100	0.31601
		1.0									−0.75659	0.14465	0.46315	−0.75656	0.14463	0.46307
		2.0									−0.61330	0.14712	0.48913	−0.61329	0.14711	0.48911
			1.0								−0.41109	0.14803	0.50317	−0.41106	0.14801	0.50315
			2.0								0.07701	0.15155	0.55698	0.07700	0.15148	0.55695
				1.0							−0.91448	0.14961	0.41747	−0.91445	0.14960	0.41746
				3.0							−0.92416	0.17035	0.41203	−0.92415	0.17040	0.41201
					0.24						−0.89268	0.14186	0.22676	−0.89266	0.14185	0.22675
					0.78						−0.91384	0.14046	0.49116	−0.91382	0.14045	0.49115
						0.5					−0.88312	0.35047	0.42254	−0.88307	0.35045	0.42252
						1.0					−0.87333	0.43293	0.42290	−0.87331	0.43291	0.42289
							1.0				−0.90632	0.14134	0.38096	−0.90630	0.14132	0.38095
							2.0				−0.90287	0.14189	0.33731	−0.90285	0.14186	0.33730
								1.0			−0.90693	0.16455	0.42211	−0.90691	0.16448	0.42210
								2.0			−0.90107	0.24083	0.42567	−0.90105	0.24081	0.42565
									0.05		−0.90490	0.13092	0.42321	−0.90489	0.13091	0.42320
									0.07		−0.90253	0.12591	0.42459	−0.90251	0.12590	0.42457
										0.05	−0.90599	0.13396	0.42250	−0.90597	0.13394	0.42249
										0.07	−0.90362	0.12949	0.42378	−0.90361	0.12947	0.42376

Method, which shows a good agreement with each other (See table 3)

DISCUSSION OF RESULTS

In this study, computation analysis is carried out via the Homotopy Analysis Method (HAM) at $20th - order$ to meet the far-field boundary conditions. This is done by holding $Bi = \lambda_T = Sr = \lambda_M = \beta = 0.1$, $Sc = 0.62$, $Pr = 0.72$, $Ra = 0.7$, $Mn = 1$, $A = B = 0.01$ constant for each varying parameter. We observed that almost all the values of the local Skin-Friction $Re_x^{\frac{1}{2}}C_f$ quantitatively displayed negative as shown in Table 3. This agreed with the expectation as the negative values justify that a drag force is exerted on the fluid by the plate which in turn impede the flow.However, the surface heat transfer significantly improve as a result of the higher values of thermal buoyancy parameter (λ_T), Prandtl number (Pr), Radiation Parameter (Ra) and Boit number

(Bi) and this consequently enhances the rate of heat transfer while the rate of mass transfer gain more strength for large values of mass buoyancy parameter (λ_M) and Schmidtl number (Sc) (see Table 3).

In figures (5–8), we observed that increase in thermal and mass buoyancy parameters (λ_T, λ_M) boost the buoyancy forces and accelerate the flow of which its aftermath effect improves the velocity of the fluid (as well as its layer thickness). The results are not the same for temperature and concentration profiles where both thermal and concentration layers thicknesses decline for large values of λ_T and λ_M. In that case, $\lambda_T > 0$ corresponds to the cooling of the plate while $\lambda_M > 0$ justify that the concentration at the plate surface is higher than the free stream concentration.

In figures (9), the influence of Prandtl number (Pr) which ranges from 0.72(Air) to 7.1(Water) is presented. It is observed from the figures that higher values of Pr due to the low thermal diffusivity diminish the average
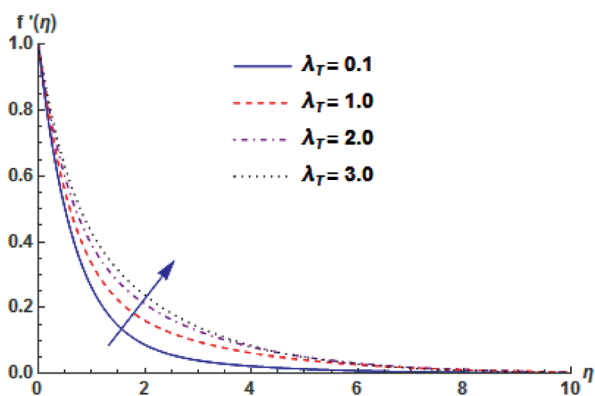

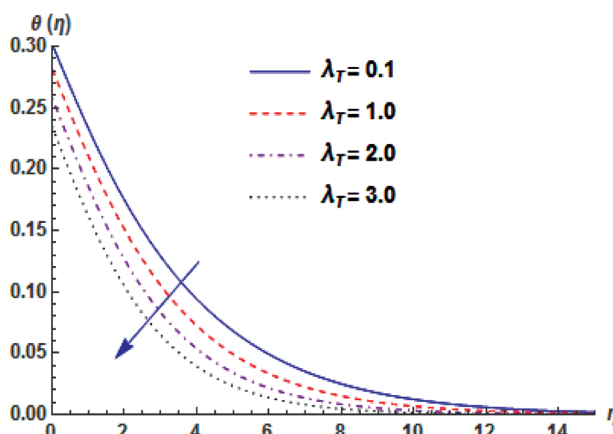**Figure 5.** Velocity profile for different values of λ_T.
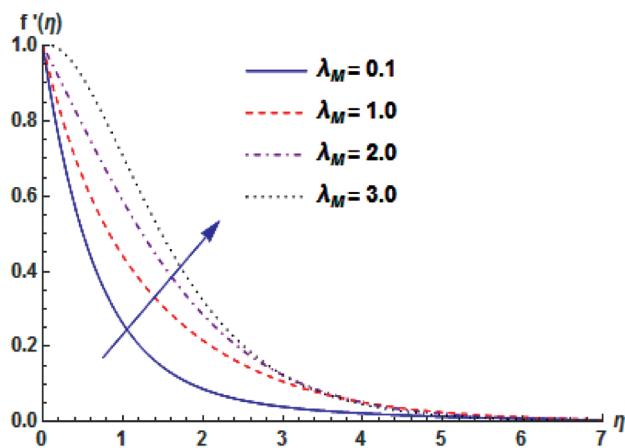

Figure 6. Temperature profile for different values of λ_T.

Figure 7. Velocity profile for different values of λ_M.
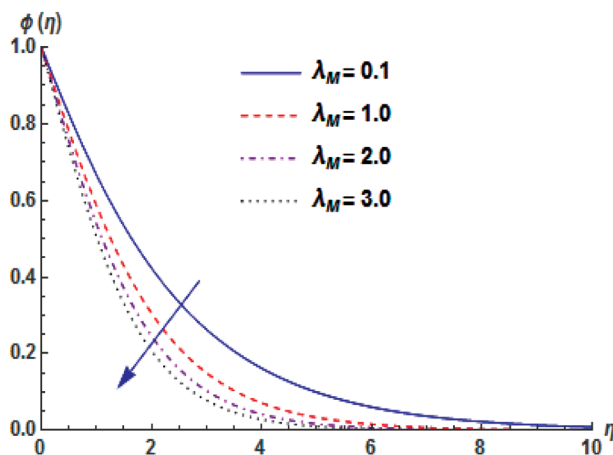

Figure 8. Concentration profile for different values of λ_M.
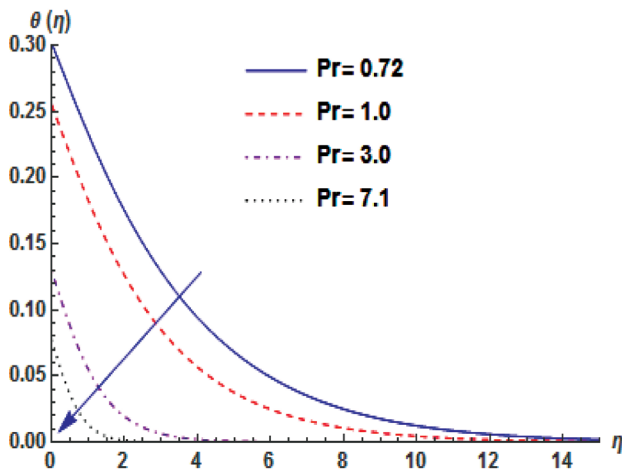
Figure 9. Temperature profile for different values of *Pr*.
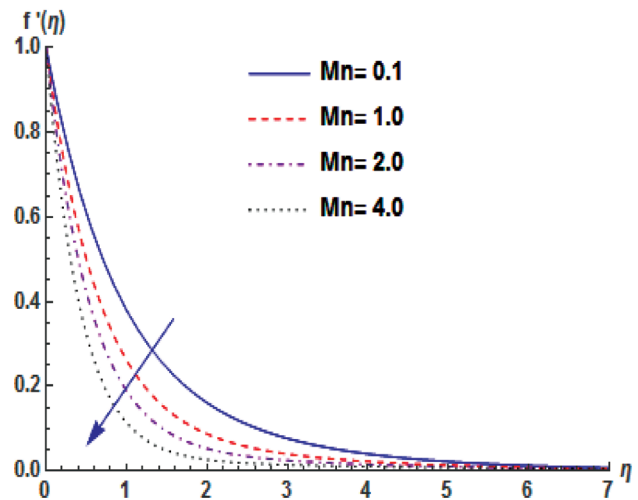

Figure 10. Velocity profile for different values of *Mn*.
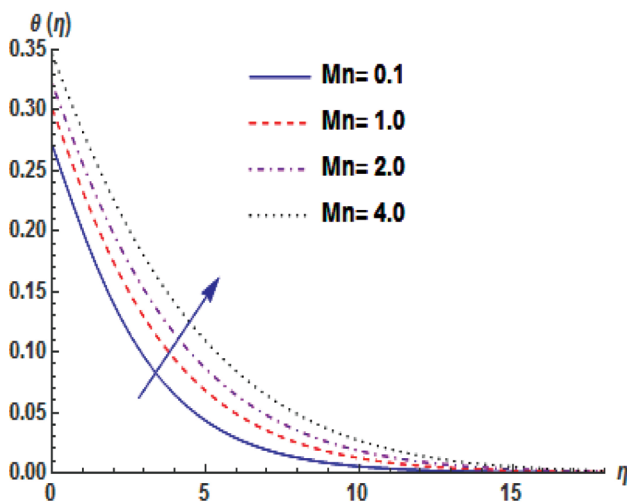

Figure 11. Temperature profile for different values of *Mn*.
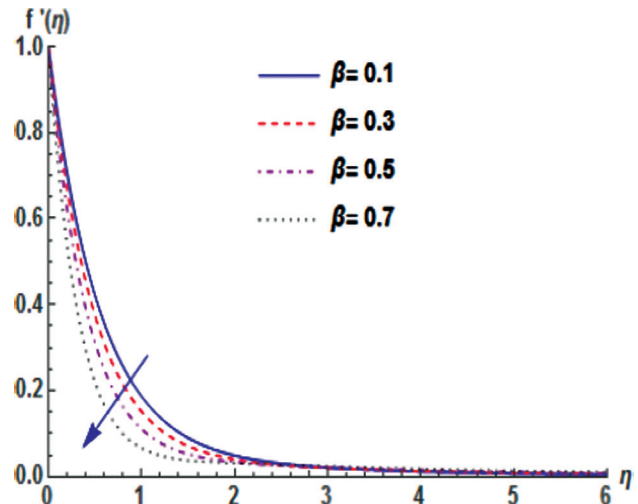

Figure 12. Velocity profile for different values of *β*.

temperature within the boundary layer which in turn reduces the momentum layer thickness. In that wise, smaller values of *Pr* enhance the thermal conductivity and enable the heat to diffuse quickly from the heated surface than higher values.

Figures (10–11) reveal the influence of magnetic interaction (*Mn*) on velocity and temperature profiles. It is noticed from fig.10 that higher values of *Mn* pioneer resistive forces called Lorentz force that resist the motion of the fluid and reduces the velocity profile and its boundary layer thickness. However, a reverse phenomenon is observed in the temperature of the fluid. An increase in *Mn* causes frictional heating across the boundary layer which increases the layer temperature of which its aftermath increases the thermal boundary layer thickness.

Figures (12–13) present the variation influence of local Weissenberg number (*β*) on velocity and temperature profiles. It is noticed from the fig. 12 that the fluid velocity decline for the large values of *β*. This result agreed with the expectation as higher values of *β* are to improve the viscoelasticity through the tensile stress which opposes the fluid velocity and reduces its layer thickness. The effect of improving viscoelasticity generates more heat within the thermal boundary layer which in turn improves the thermal layer thickness.

The effect of Schmidtl number for most encountered chemical in the application is varied in Figure 14 on concentration field. At higher values of *Sc*, the diffusion properties of the fluid experienced downfall which in turn falls the concentration profile near the boundary layer as well as
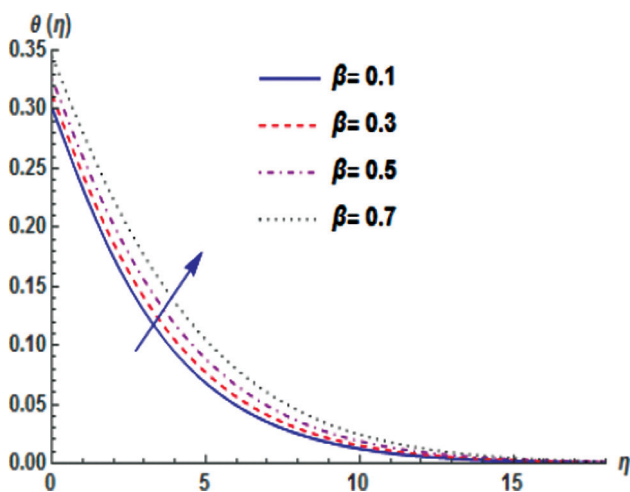
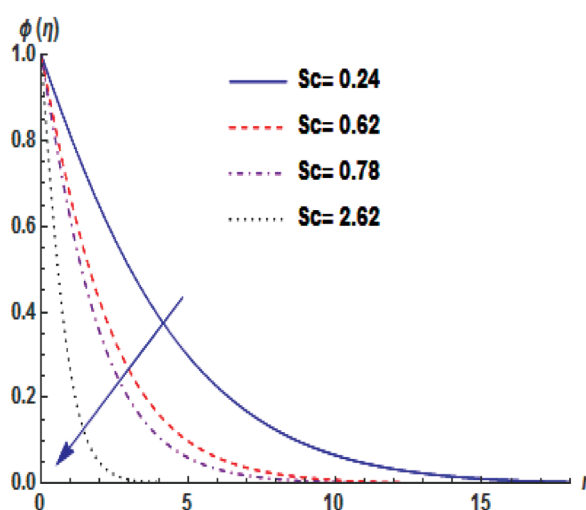**Figure 13.** Temperature profile for different values of β.

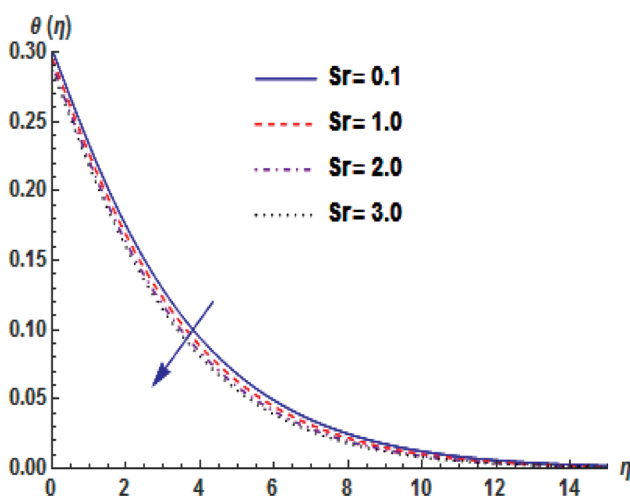**Figure 14.** Concentration profile for different values of Sc.

Figure 15. Temperature profile for different values of Sr.
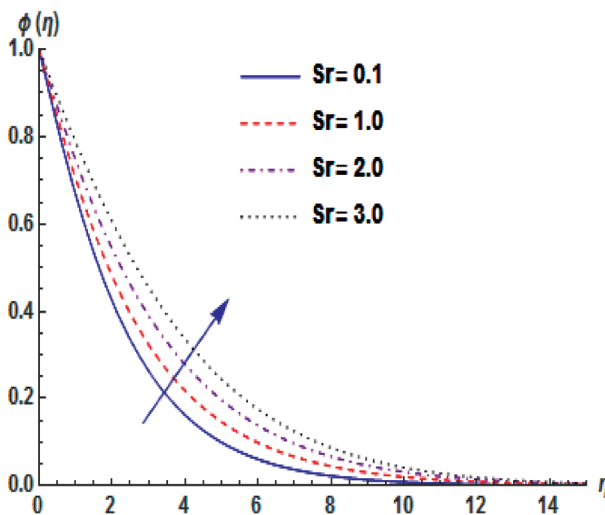
Figure 16. Concentration profile for different values of Sr.

concentration boundary layer thickness (See Akinbo and Olajuwon [32]).

Figures (15–16) present the effect of Soret Number (Sr) on temperature and concentration profiles. Physically, we observed from figure 15 that an increase in Sr contributes to the falling of the temperature which ultimately reduces the thermal boundary layer thickness. However, the opposite phenomenon is observed in the concentration field which ultimately boosts concentration boundary layer thickness (see Fig. 16).

Figure 17 addresses the influence of the radiation parameter (Ra) on the temperature profile. It is noticed that the temperature of the fluid improves due to the increasing

values of Ra. This is true as higher values of Ra magnify the conduction of heat transfer to thermal heat transfer of which its aftermath effect strengthens the thermal boundary layer thickness.

Figures (18–19) presents the influence of the internal heat generation/absorption parameter $(A,B) > 0$ on the temperature profile. As expected, an increase in (A,B) corresponds to the enhancement of more heat within the layer, which in turns improves the temperature of the fluid and strength the thermal boundary layer thickness

Figure (20) presents the influence of Boit Number (Bi) on the temperature profile. An increase in Bi constitutes strong convective heating within the boundary which
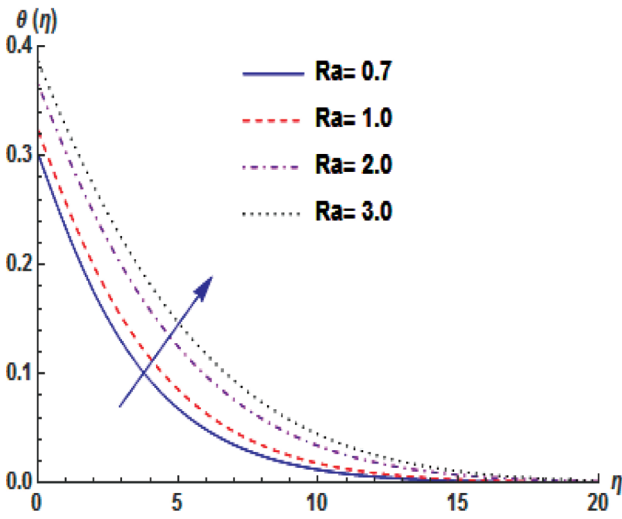
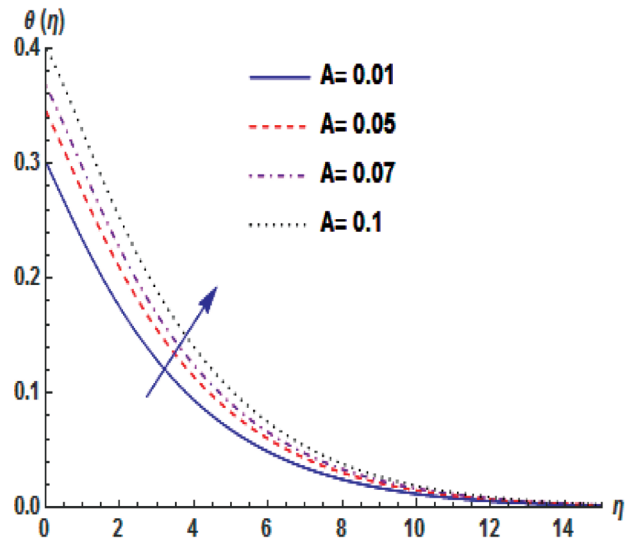**Figure 17.** Temperature profile for different values of *Ra*.

Figure 18. Temperature profile for different values of *A*.
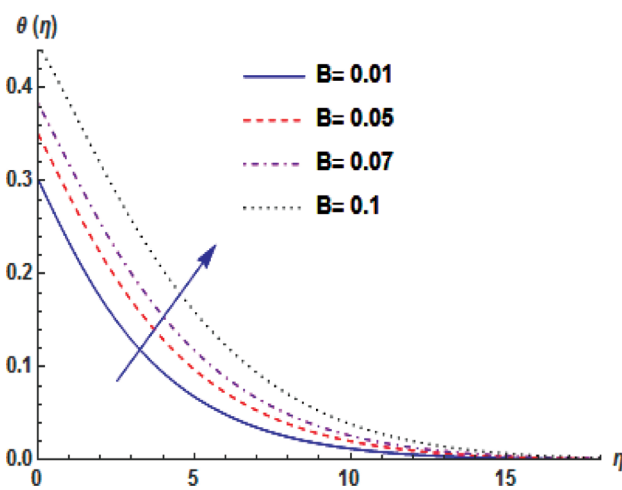

Figure 19. Temperature profile for different values of *B*.
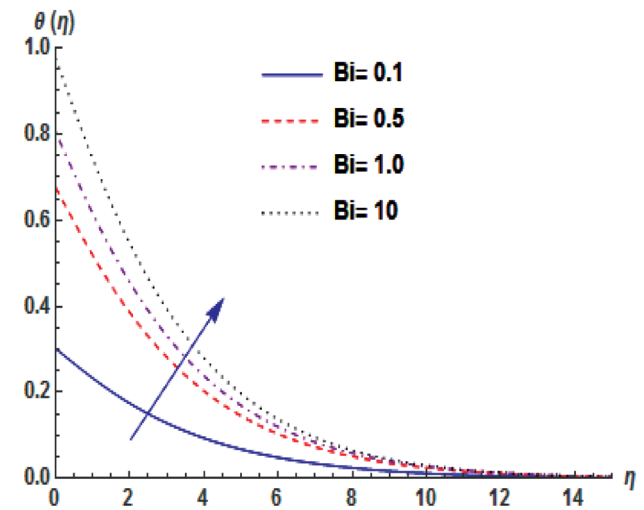

Figure 20. Temperature profile for different values of *Bi*.

ultimately maximizes the thermal boundary layer thickness. However, this enhancement paves way for the penetration of thermal effect to the quiescent fluid.

CONCLUSION

In this work, Homotopy Analysis Method is employed to solve the three dimensionless equations corresponding to momentum, energy, and concentration which describe the influence of Convective Boundary Condition on heat and mass transfer in Walters' B fluid over a vertical plate with thermal-diffusion effect. The results of various embedded parameters are analyzed through graphs and tables. The following conclusions were drawn from the results obtained

- Setting $\beta = 0$, Walters' B model behaves like an ordinary Newtonian fluid
- The skin-friction quantitatively displayed negative, indicating that the drag forces are exerted on the fluid by the plate which in turns impede the flow
- Higher values of (A,B) enhance the temperature which in turn pioneer the lightening of the surface and enable the fluid to flow faster.
- The tensile stress effect is magnified for large values of Weissenberg number which ultimately declines the velocity boundary layer thickness.
- The temperature distribution and surface heat transfer are boosted when Radiation intensity improves.
- Large values of Biot number magnifies thermal effect and allow its penetration to the quiescent

fluid. The strength of the Biot number contributes to the drying of the materials component in the Engineering field.

Compliance with ethical standards

Conflict of interest: The authors declare that they no conflict of interest.

NOMENCLATURE

Mn Magnetic field
β local Weissenberg Number
λ_T Thermal buoyancy parameter
λ_M Mass buoyancy parameter
Bi Biot number
Pr Prandtl number,
Ra Radiation parameter
Sc Schmidtl number
A space-dependent heat generation/absorption
B Temperature-dependent heat generation/Absorption
Q_0 non-uniform heat generation/absorption Coefficient
D_m mass diffusivity

Greek symbols
α thermal diffusivity
β_c concentration expansion coefficient
η Similarity variable
θ dimensionless temperature
ν kinematic viscosity
ψ Stream Function
ρ density
q_r Radiation heat flux
C_p specific heat at constant pressure
β_T temperature expansion coefficient
g acceleration due to gravity
σ fluid electrical conductivity
h_f heat transfer coefficients

ACKNOWLEDGMENT

The authors would like to thank the reviewers and anonymous referees for their useful suggestions that led to definite improvement in the paper.

AUTHORSHIP CONTRIBUTIONS

Concept: Design: Materials: Data Analysis: Literature search: Writing; Critical revision:

DATA AVAILABILITY STATEMENT

No new data were created in this study. The published publication includes all graphics collected or developed during the study.

CONFLICT OF INTEREST

The author declared no potential conflicts of interest with respect to the research, authorship, and/or publication of thisarticle.

ETHICS

There are no ethical issues with the publication of this manuscript.

REFERENCES

[1] Ali MM, Chen TS, Armaly, BF. Natural Convection-Radiation interaction in boundary layer flow over horizontal surfaces. AIAA Journal 1984;22:1797–803. [CrossRef]

[2] Arpaci VS. Effect of thermal radiation on the laminar free convection from a heated vertical plate International Journal of Heat and Mass Transfer 1968;11:871–81. [CrossRef]

[3] Afify AA, El-Aziz MA. Lie group analysis of flow and heat transfer of non-Newtonian nanofluid over a stretching surface with convective boundary condition. Pramana 2017;88:31. [CrossRef]

[4] Sarafraz MM, Hormozi F, Kamalgharibi M, Sedimentation and convective boiling heat transfer of CuO-water/ethylene glycol nanofluids. Heat Mass Transfer 2014;50:1237–49. [CrossRef]

[5] El-Aziz MA, Nabil T. Effect of time-dependent heat source/sink on slip flow and heat transfer from a stretching surface with homotopy analysis method. Meccanica 2015;50:1467–80. [CrossRef]

[6] El-Aziz MA. Thermal-diffusion and diffusion-thermo effects on combined heat and mass transfer by hydromagnetic three-dimensional free convection over a permeable stretching surface with radiation. Physics Letters A 2008;372:263–72. [CrossRef]

[7] El-Aziz MA. Radiation effect on the flow and heat transfer over an unsteady stretching sheet. International Communications in Heat and Mass Transfer 2009;36:521–4. [CrossRef]

[8] Abo-Eldahab EM, El-Aziz MA. Blowing/suction effect on hydromagnetic heat transfer by mixed convection from an inclined continuously stretching surface with internal heat generation/absorption. International Journal of Thermal Sciences 2004;43:709–19. [CrossRef]

[9] Oahimire JI, Olajuwon BI. Effects of radiation absorption and thermo-diffusion on MHD heat and mass transfer flow of a micro-polar fluid in the presence of heat source. Application and Applied Mathematics 2014;9:763–79.

[10] Makinde OD. On MHD heat and Mass Transfer over a moving vertical plate with a corrective surface

boundary condition, Can J Chem Eng 2010;88:983–90. [CrossRef]

[11] El-Aziz MA. The effects of variable fluid properties and viscous dissipation on forced convection of viscoelastic liquids in a thin film over an unsteady stretching sheet. Can J Phys 2010;88:607–16. [CrossRef]

[12] Labropulu F, Husain I, Chinichian M. Stagnation-point flow of the Walters' B' fluid with slip, International Journal of Mathematics and Mathematics Science 2004;61:3249–58. [CrossRef]

[13] Shivakumara IS, Lee J, Malashetty MS, Sureshkumar S. Effect of thermal modulation on the onset of convection in walters b viscoelastic fluid-saturated porous medium. Transp Porous Med 2011;87:291–307. [CrossRef]

[14] Rana GC, Kango SK, Chadha K. Magneto-thermal convection in Walters' (Model B') elastico-viscous fluid saturated by a Darcy-Brinkman porous medium. Engineering Mechanics 2014;21:425–35.

[15] Aggarwal AK, Verma A. The effect of compressibility, rotation and magnetic field on thermal instability of walters'B fluid permeated with suspended particles in porous medium. Thermal Science 2014;18:S539–50. [CrossRef]

[16] Pandey SD, Nema VK, Sanddep T. Charateristic of Walter's B visco-elastic nanofluid layer heated from below. International Journal of Energy Engineering 2016;6:7–13.

[17] Thirumurugan K, Vasanthakumari R. Double – diffusive convection of non - newtonian Walters' (MODELB′) viscoelastic fluid through brinkman porous medium with suspended particles. International Journal of Heat and Technology 2016;34:357–63. [CrossRef]

[18] Sharma V, Rana GC, Kumar S. Stability of stratified Walters' (Model B') fluid in porous medium in the presence of suspended particles and variable magnetic field. Jnanabha 1998;28:97–110.

[19] Kango SK, Singh V, Rana GC. Thermosolutal instability in Walters' (model B') fluid in the presence of Hall currents in porous medium in hydromagnetics. Journal of Indian Mathematical Society 2011;78:65–77.

[20] Rana GC. The onset of convection in Walters' (model B') elastico-viscous fluid in a Darcy-Brinkman porous medium. Journal of Pure Applied and Industrial Physics 2012;2:55–62.

[21] Rana GC, Jamwal HS. Effect of rotation on the onset of compressible viscoelastic fluid saturating a darcy-brinkman porous medium. Engineering Mechanics 2012;19:445–55.

[22] Nadeem S, Mehmood R, Motsa SS. Numerical investigation on MHD oblique flow of Walter's B type nanofluid over a convective surface. International Journal of Thermal Sciences 2015;92:162–72. [CrossRef]

[23] Mishra SR, Baag S, Bhatti MM. Study of heat and mass transfer on MHD Walters'B nanofluid flow induced by a stretching porous surface. Alexandria Engineering Journal 2018;57:2435–43. [CrossRef]

[24] Hayat T, Asad S, Mustafa M, Hamed HA. Heat transfer analysis in the flow of Walters' B fluid with a convective boundary condition. Chin Phys B 2014;23:084701–1. [CrossRef]

[25] Uddin J, Bég OA, Ismail AI. Radiative convective nanofluid flow past a stretching/shrinking sheet with slip effects. Journal of Thermophysics and Heat Transfer 2015;27:513–23. https://doi.org/10.2514/1.T4372

[26] Almakki M, Mondal H, Sibanda P. Entropy Generation in MHD flow of viscoelastic Nanofluids with Homogeneous-Heterogeneous reaction, partial slip and nonlinear thermal radiation. Journal of Thermal Engineering 2020;6:327–45. [CrossRef]

[27] Liao SJ. On the analytic solution of magnetohydrodynamic flows of non-Newtonian fluids over a stretching sheet. J Fluid Mech 2003;488:189–212. [CrossRef]

[28] Akinbo BJ, Olajuwon BI. Homotopy analysis investigation of heat and mass transfer flow past a vertical porous medium in the presence of heat source. International Journal of Heat and Technology 2019;37:899–908. [CrossRef]

[29] Hayat T, Qayyum S, Alsaedi A, Ahmad B. Magnetohydrodynamic (MHD) nonlinear convective flow of Walters, B nanofluid over a nonlinear stretching sheet with variable thickness. International Journal of Heat and Mass Transfer 2017;110:506–14. [CrossRef]

[30] Olubode KK, Tosin O, Adeola JO, Isaac LA. Homotopy analysis of MHD free convective micropolar fluid flow along a vertical surface embedded in non-darcian thermally-stratified medium. Open Journal of Fluid Dynamic 2016;6:198–221. [CrossRef]

[31] Liao SJ. Beyond Perturbation: An Introduction to Homotopy Analysis Method. Boca Raton, Florida: Chapman and Hall; 2003

[32] Akinbo BJ, Olajuwon BI. Convective heat and mass transfer in electrically conducting flow past a vertical plate embedded in a porous medium in the presence of thermal radiation and thermo diffusion. Computational Thermal Sciences 2019;11:367–85. [CrossRef]